EPSC Abstracts
Vol. 11, EPSC2017-173, 2017
European Planetary Science Congress 2017

A PREVIEW OF IMAGING CAPABILITY OF CHANG'E-5 LUNAR REGOLITH PENETRATING RADAR

J. Feng, Y. Su, S. Dai, S. Xing, C. Ding, Y. Xiao and C. Li
Key Laboratory of Lunar and Deep Space Exploration, National Astronomical Observatories, Chinese Academy of Sciences, Beijing 100012, China (suyan@nao.cas.cn)

Abstract

This article present the work principle and data processing method of Lunar Regolith Penetrating Radar (LRPR) on *Chang'e-5* (CE-5) Lander. It can be a reference for scientist who will use LRPR data to reveal the regolith structure at the landing site.

1. Introduction

The Chinese *Chang'e-5* (CE-5) mission will be the first lunar sample return mission in 40 years. An instrument named the Lunar Regolith Penetrating Radar (LRPR) will be carried by the CE-5 lander to investigate the structure of the regolith under the spacecraft. These results will be used to guide the sample drilling process. The LRPR transmits carrier-free pulses with a working frequency range of 1-3 GHz. In contrast to Lunar Penetrating Radar (LPR) on board the *Chang'e-3 Yutu* rover, the LRPR is a fixed antenna array (Figure 1). To assess and improve the detection of the instrument, a series of ground tests were performed over the last two years. A 7 m × 3 m × 2.5 m concrete pool filled with regolith simulant was built as the test field. Various objects such as granite slate, basalt rocks and metallic balls were placed within the regolith simulant. The lander model was surrounded by electromagnetic absorbing material (EAM) during these tests.

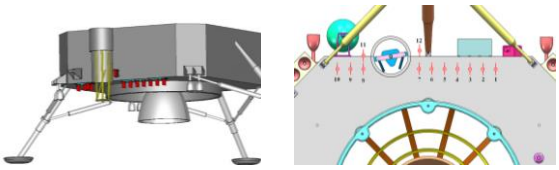

Figure 1: The lander model ground test setup. The LRPR is installed by one edge of the lander model's bottom, consisting of 12 separate antennas.

2. Experiment data

The LRPR is a multi-offset radar and its data processing is different from the traditional generic common-offset ground penetrating radar (GPR). The 12 antennas work in turn to send or receive radar signals, giving 132 traces of data record at one test. The first 11 traces are signals sent by antenna #1 and received by the other 11 antennas, and so on. The raw data does not only contain the echoes caused by objects buried in the regolith but also the multiple reflections between lander and regolith surface and reflections from the lander itself. In order to eliminate these signal contaminations, we measured a 'background' by covering the regolith surface with EAMs.

Initially, bandpass filtering is applied to both the raw data and the 'background' data to remove system noise. Then we subtract the 'background' from the raw data to achieve further background removal. The filtered data is a cleaner radargram with little clutter. It is difficult to observe hyperbolic patterns usually seen in the traditional GPR, due to the special data characteristics, complicating objects recognition (Figure 2).

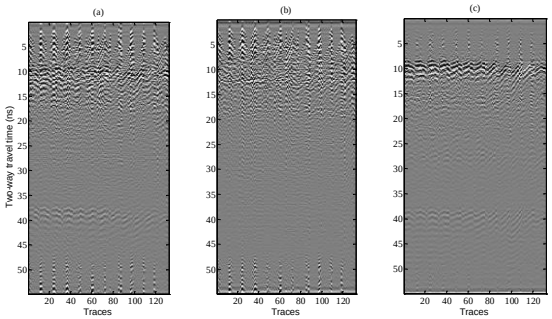

Figure 2: (a) and (b) are the raw data and the 'background' after bandpass filtering. (c) is the radargram after background removal.

3. Velocity estimation

Before applying migration to the data, we use the velocity spectrum method to estimate the propagation velocities. This method is based on the cross-correlation of the traces in a common middle point (CMP) gather [1-3] and it could be used for velocity analysis of radar data for stratified media [4]. Although the LRPR has several CMP gathers, we treat them as one because the regolith simulant is homogenous and its top and bottom are flat. The unnormalized cross-correlation sum is calculated within a time gate that follows a specific path across the CMP gather. The shape of the path is determined by a root-mean-square (RMS) velocity. Figure 3 shows the velocity spectrum at different travel time ranges. From the velocity spectrum, we can pick two RMS velocities just by looking for the peak value of the contour. Then the Dix equation is used to calculate an interval velocity in the regolith [5].

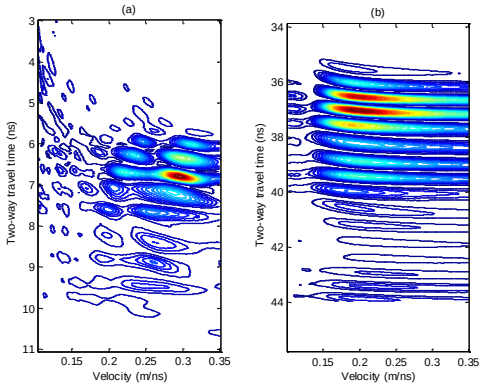

Figure 3: The velocity spectrum for travel time 3-11 ns (a) and 34-46 ns (b). The peak value in (a) is the RMS velocity from the radar to the regolith surface, and the peak value in (b) is the RMS velocity from the radar to the regolith bottom.

4. Migration result

We use the Diffraction Stack Migration method to migrate the LRPR data. A regolith simulant grid is built. Each cell of the grid has a size of 1 cm × 1 cm and all the cells have an initial value of zero. Then we calculate the value of the cells by using the followed function:

$$C_i = \sum_{j=1}^{132} A_{j,t(i)}$$

Where i is the cell number, $A_{j,t(i)}$ is the amplitude value on the jth trace at $t(i)$. $t(i)$ is the two-way travel time from the transmitting antennas via the ith grid to the receiving antennas. Coordinates of the anttenas and grids' positions are used to determine the propagation geometry and travel distances. In this process, the Snell law is also considered. A migrated radargram is derived after all the cells in the grid finish their accumulation (Figure 4).

Comparing the migration result and the profile section of the test field (Figure 4), it is observed that the interface between regolith and air and metallic bottom can be successfully recognized. Also, the target *a* and *b* are distinguishable, but some clutter in the shallow depth still exists and remains difficult to remove.

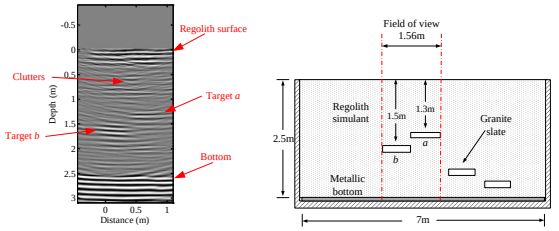

Figure 4. The migration result of the LRPR data and diagram of profile section of the test field.

5. Conclusions and Future Work

With this method, the structure of the regolith simulant under the lander is revealed to some degree. However, we need to exercise caution when interpreting the characteristics at shallow depth (up to 1 m) due to artifact. As a future endeavour, Kirchhoff migration [2, 3] or reverse time migration method will be used to improve these results.

Acknowledgements

This work is funded by the National Natural Science Foundation of China (Grant Nos. 41403054 and 11173038) and the China Scholarship Council (201604910333).

References

[1] Yilmaz, Ö. (1989) *Geophysical Prospecting*, *37*, 357. [2] Feng, X. and Sato, M. (2004) *Inverse problems*, *20*, S99. [3] Sato, M. and Feng, X. (2005) *APSIS IEEE*, 206-209. [4] Greaves, R. J. et al. (1996) *Geophysics*, *61*, 683. [5] Dix, C.H. (1955) *Geophysics*, *20*, 68-86.